1-5-2021

Immobilization of cesium and iodine into $Cs_3Bi_2I_9$ perovskite-silica composites and core-shell waste forms with high waste loadings and chemical durability

Kun Yang
Rensselaer Polytechnic Institute

Weiguang Zhu
Rensselaer Polytechnic Institute

Spencer Scott
Savannah River National Laboratory

Yachun Wang
Rensselaer Polytechnic Institute

Jianwei Wang
Louisiana State University

See next page for additional authors

Recommended Citation

Yang, K., Zhu, W., Scott, S., Wang, Y., Wang, J., Riley, B., Vienna, J., & Lian, J. (2021). Immobilization of cesium and iodine into $Cs_3Bi_2I_9$ perovskite-silica composites and core-shell waste forms with high waste loadings and chemical durability. *Journal of Hazardous Materials, 401* https://doi.org/10.1016/j.jhazmat.2020.123279

Journal of Hazardous Materials 401 (2021) 123279

Contents lists available at ScienceDirect

Journal of Hazardous Materials

journal homepage: www.elsevier.com/locate/jhazmat

Immobilization of cesium and iodine into $Cs_3Bi_2I_9$ perovskite-silica composites and core-shell waste forms with high waste loadings and chemical durability

Kun Yang[a], Weiguang Zhu[a], Spencer Scott[b], Yachun Wang[a], Jianwei Wang[c], Brian J. Riley[d], John Vienna[d], Jie Lian[a,*]

[a] Department of Mechanical, Aerospace and Nuclear Engineering, Rensselaer Polytechnic Institute, NY 12180, United States
[b] Savannah River National Laboratory, Aiken, SC 29801, United States
[c] Department of Geology and Geophysics, Louisiana State University, LA 70803, United States
[d] Pacific Northwest National Laboratory, Richland, WA 99354, United States

GRAPHICAL ABSTRACT

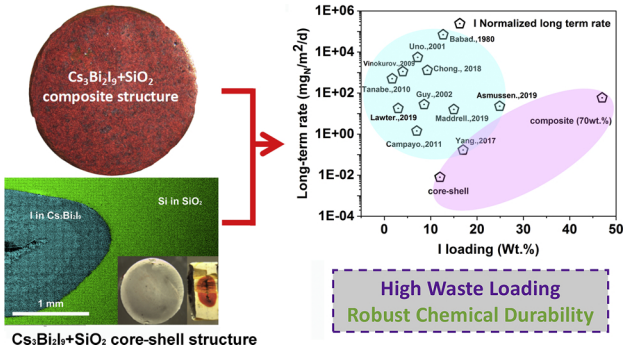

ARTICLE INFO

Editor: L. Eder

Keywords:
Pervoskite
Fission product
Silica
Waste form
Sparking plasma sintering

ABSTRACT

$Cs_3Bi_2I_9$, a defect perovskite derivative, is a potential host phase to immobilize iodine and cesium with high waste loadings. In this work, two strategies were explored to form $Cs_3Bi_2I_9$-silica composites and a core-shell structure in order to improve chemical durability of waste form materials meanwhile maintaining high waste loadings. $Cs_3Bi_2I_9$ loadings as high as 70 wt.% were incorporated into a silica matrix to form silica-ceramic composites, and 20 wt.% $Cs_3Bi_2I_9$ was encapsulated into silica to form a core–shell structure by low temperature spark plasma sintering. Chemical durability of the composite and core-shell waste forms was evaluated by semi-dynamic leaching experiments, and Cs and I were incongruently released from waste form matrices. A BiOI alteration layer formed, acting as a passivation layer to reduce the release of radionuclides. The long-term iodine release rate was low (30 mg m^{-2} day^{-1}) for the 70 wt.% $Cs_3Bi_2I_9$–silica composite leached in deionized water at 90 °C, which can be further reduced to 5×10^{-3} mg m^{-2} day^{-1} for the 20 wt.% core-shell structure. This work highlights a robust way to immobilize the highly mobile radionuclides with high waste loadings through encapsulation into durable matrices and a surface passivating mechanism that can greatly reduce the elemental transport from waste form materials and significantly enhance their chemical durability.

* Corresponding author.
E-mail address: LIANJ@rpi.edu (J. Lian).

https://doi.org/10.1016/j.jhazmat.2020.123279
Received 31 March 2020; Received in revised form 16 June 2020; Accepted 17 June 2020
Available online 22 June 2020

1. Introduction

Effective management of radioactive iodine and cesium, two key problematic and highly mobile fission products from the chemical reprocessing of used nuclear fuels, is critical for the development of safe and sustainable nuclear fuel cycles. Among these, short-lived Cs-137 is one of the major heat and dose generators during the initial storage of the waste. Long-lived Cs-135 and I-129 are major dose contributors for the long-term disposition of nuclear wastes. Isotopes Cs-135 and Cs-137 are difficult to immobilize because of their high radiotoxicity and water solubility (Carter et al., 2002). Cs-135 presents a long-term disposal challenge with a long half-life ($t_{1/2}$ = 2.3 × 10^6 yr). The long-lived isotope I-129 ($t_{1/2}$ = 1.6 × 10^7 yr) is also highly mobile in gas streams and aqueous solutions (Riley et al., 2016), and one of the most-widespread radionuclides in the Hanford groundwater systems (Brown et al., 2007; Muller et al., 2014). Both Cs and I are volatile at temperatures typical for radioactive waste immobilization.

Current capture and immobilization methods include precipitation, caustic scrubbing, ion exchange, adsorption, reverse osmosis, and ultrafiltration (Haefner and Tranter, 2007; Ambashta and Sillanpaa, 2012). The leading technology for iodine capture is based on Ag-based absorbents, particularly Ag-exchanged mordenite (Ag°Z) (Haefner and Tranter, 2007; Ambashta and Sillanpaa, 2012; Krumhansl and Nenoff, 2011), which are effective in removing both organic and inorganic iodine from off-gas process streams. Additional solid absorbents were developed including Ag-functionalized silica aerogels (Sinha et al., 1995; Matyas et al., 2011; Riley et al., 2017), graphene powders and aerogels (Scott et al., 2015) and sulfur-based chalcogels (Matyas et al., 2011). However, the utilization of Ag is an environmental concern and does not meet the EPA standards under Resource Conservation and Recovery Act (RCRA) for land disposal (Haefner and Tranter, 2007; U.S.E.P.A., 2012). Besides, involving the silver flask into the waste forms will also significantly increase the cost. For the capture of cesium, synthetic zeolite has been applied for the removal of cesium from actual radioactive liquid waste (Sinha et al., 1995). The adsorption of Cs onto the porous zeolite is a reversible process, and Cs-137 can be released back into the environment at elevated environmental temperatures (Moore et al., 2019).

Following removal of radioactive iodine from off-gas and cesium from liquid streams, these isotopes need to be incorporated into durable waste forms with high chemical durability. The current baseline waste form for reprocessing high-level wastes is borosilicate glass. However, very limited iodine (typically less than 1 wt.% and the maximum loading is 2.4 wt.%) can be incorporated into borosilicate glass because of its low solubility in the glass matrix and high volatility during the high temperature vitrification process (Riley et al., 2016; Muller et al., 2014). Ceramic waste forms based on an apatite structure-type (with a general chemical formula of $M_{10}(XO_4)_6Y_2$ with M = Pb,Ca; X = P,V; Y = I) were proposed as promising waste form phases for iodine incorporation (Zhang et al., 2018a, 2018b). For instance, iodate-hydroxyapatite with 7 wt.% loading and dense lead-vanadate iodoapatite $Pb_5(VO_4)_3I_{1-x}$ (x = 0−0.15) (in general 5−7 wt.%) have been synthesized and leaching tests in pure water at 90 °C reported high iodine release rates (Campayo et al., 2011; Guy et al., 2002). Ceramic waste forms with enhanced waste loadings and chemical durability were also developed for Cs immobilization. Hollandite with a general form of $A_xB_yC_{8-y}O_{16}$, such as $(Ba,Cs)(Al,Ti)_2Ti_6O_{16}$, a phase of Synroc, has been recognized as a promising host phase for the immobilization of Cs (Carter et al., 2002). Other types of hollandite including $Ba_{1.15-x}Cs_{2x}Cr_{2.3}Ti_{5.7}O_{16}$ and $Cs_{0.1}Ba_{1.0}(Ti_{0.6}Al_{1.5})^{3+}Ti_{5.0}O_{16}$ (Luca et al., 2005; Tumurugoti et al., 2018) were synthesized with controlled amounts of Cs by altering the trivalent cation in the tunnel (*e.g.*, Al, Fe, Ga), and their leaching behavior in both water and acid solution was evaluated (Luca et al., 2005; Tumurugoti et al., 2018; Grote et al., 2019; Amoroso et al., 2014).

Inorganic Pb-free metal halide perovskite-based derivatives such as Cs_2SnCl_6 and $Cs_3Bi_2I_9$ display high defect tolerance and less toxicity than lead halides. Cs_2SnCl_6 has long been used for the separation of Cs-135 and Cs-137 from the liquid stream of reprocessing of spent nuclear fuels (Geoking et al., 1963; Kalaiselvan and Prasad, 1988), and could be a promising waste form material due to very high loadings of Cl (Zhu et al., 2019). The $Cs_3Bi_2I_9$ structure consists of identical pervoskite-like fragments with alternating edge sharing $[BiI_6]^{3-}$ octahedral layers, where the voids are filld with Cs^+ cations (Sun et al., 2018). Similar to Cs_2SnCl_6, $Cs_3Bi_2I_9$ has very high Cs and I loadings up to 20 and 60 wt. %, respectively, significantly higher than these in the conventional waste forms such as hollandite, apatite, and borosilicate glass. Despite high waste loadings, $Cs_3Bi_2I_9$ has not been reported previously as a potential nuclear waste form yet due to its relatively-high solubility (2 g L^{-1}) in water and low chemical durability (Davies, 1973). New design of the waste form matrices and synthesis of materials with high waste loadings and acceptable chemical durability are highly desired to further explore the potential of using $Cs_3Bi_2I_9$ as a host phase for iodine and Cs immobilization.

In this work, we explore two strategies based on $Cs_3Bi_2I_9$-silica composites or a core-shell structure in which silica is used as a matrix to encapsulate cation-deficient defect perovskite $Cs_3Bi_2I_9$ with high Cs and I loadings. The $Cs_3Bi_2I_9$ powders were synthesized through a solution-based co-precipitation method followed by thermal consolidation. Dense waste forms can be fabricated at relatively lower temperatures and high pressure by spark plasma sintering (SPS). Semi-dynamic dissolution experiments were performed and the long-term leaching behavior of the composites and core–shell structures were evaluated in deionized water under room temperature and 90 °C for 14 days. The current study is to investigate the chemical durability and elementary releasing behavior of defect perovskite $Cs_3Bi_2I_9$ in composites and core–shell structures, further providing scientific insight into the design of the waste form.

2. Materials and methods

2.1. Synthesis of defect $Cs_3Bi_2I_9$

Defect perovskite $Cs_3Bi_2I_9$ was first synthesized through a solvent volatilized crystallization (SVC) method as reported by Zhang et al. (2018a) and (2018b) at a temperature lower than 80 °C (Zhang et al., 2018a, 2018b). Here, CsI (Sigma Aldrich) and BiI_3 (Sigma Aldrich) powders were utilized as precursor materials to simulate the radioactive cesium and iodine waste materials with a molar ratio of 3:2. Both powders were dispersed in dimethylformamide (DMF) (Alfa Aesar) with a weight to volume ratio (gram:ml) of 1:5 by vigorously stirring the mixture for 30 min. with a stirring speed of 300 rpm, followed by low-speed 80-rpm stirring for 24 h at 80 °C until the DMF was fully evaporated. The powder mixture was then oven dried overnight at 80 °C to obtain the final product shown as dark red powders. Silica gel powders, purchased from Sigma-Aldrich with a particle size of 300 μm, were ball milled to reduce the particle size to approximately 3 μm by a high-energy ball milling (Fritsch, UK). The ball-milling speed was set as 500 rpm for four cycles at 30 min/cycle. For the composite structure, variable amounts of $Cs_3Bi_2I_9$ powders ranging from 30 to 70 wt.% were mixed with silica gel powders with a mortar and pestle, followed by SPS consolidation.

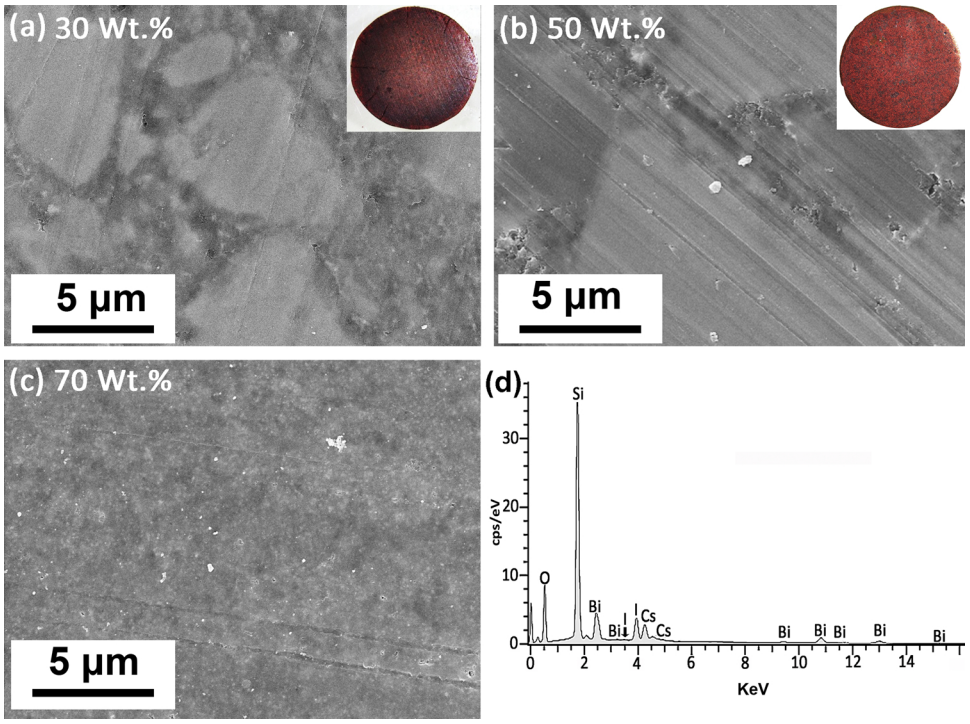

Fig. 1. Scanning electron microscopy (SEM) images and EDS showing microstructure and micro-chemical analysis of the $Cs_3Bi_2I_9$-silica composites with different $Cs_3Bi_2I_9$ (wt.%): (a) 30 %, (b) 50 %, (c) 70 % of $Cs_3Bi_2I_9$; and (d) an EDS spectrum of the 70 wt.% composite. Insets on (a) and (b) are photographs which show the composite waste form pellets corresponding to 30 wt.% and 50 wt.% $Cs_3Bi_2I_9$.

2.2. Spark plasma sintering consolidation of composite and core-shell structures

The SPS consolidation was completed using a Model 10−3 SPS system (Thermal Tech. LLC, Santa Rosa, CA), and one-step sintering process was applied for consolidating $Cs_3Bi_2I_9$/silica composites, as shown in Supplemental Materials Fig. s1a, and the detailed procedure was demonstrated in Supplemental Materials. The core–shell structure was consolidated by a two-step process and the detailed consolidation process was detailed in Supplemental Fig. s1b and 1c. $Cs_3Bi_2I_9$ powders were first consolidated into a 6 mm diameter pellet based on the process shown in Supplemental Fig. 1b. The pre-consolidated $Cs_3Bi_2I_9$ pellet was placed into a large-sized graphite die (10 mm in diameter) with two layers of silica powders. By encapsulating the pre-formed pellets into silica powders, and SPS consolidation, the core-shell structure can form with $Cs_3Bi_2I_9$ as the core and silica shells surrounding the inner pellet to form the core-shell structure. The SPS sintering route was shown in Supplemental Fig. s1c. During SPS consolidation, a steady argon flow with a flow rate of 1 L min^{-1} was purged into the chamber in order to avoid the possible oxidation and degradation of $Cs_3Bi_2I_9$ and graphite die during the SPS consolidation.

2.3. Sample crystalline structure and microstructure characterization

The dried powders and as-sintered pellets were characterized using a XRD with a Panalytical X'Pert Pro system (Westborough, MA, USA) using a copper target (K_α = 0.15406 nm) and a step size of 0.0131° 2θ. SEM was conducted using an FEI Versa (USA) with energy dispersive spectroscopy (EDS) conducted with an additional Oxford Instruments (Abingdon, UK) INCA detector. Theoretical density measurements of the pellets were carried out using an Adam analytical scale (Danbury, NY, USA). Surface of the samples before and after the leaching experiments were characterized by the Raman shift, which was measured with a Raman spectrometer using a 514-nm green laser with an exposure time of 10 s with three-times average at an operating power of 20 mW. Thermal stability was determined by a thermogravimetric analysis (TGA) system using a TGA-Q50 (TA instruments, New Castle, DE) with small pieces of pellets with masses of ~20 mg placed in an alumina crucible under a steady argon flow (flow rate = 50 mL min^{-1}). The temperature was gradually increased to 1100 °C at a rate of 20 °C min^{-1} during testing, followed by decreasing the temperature from 1100 °C to 50 °C with the same cooling rate.

2.4. Chemical durability tests with semi-dynamic leaching experiments

Fourteen days of semi-dynamic leaching experiments were conducted for both composite and core-shell pellets in high-purity 18-MΩ deionized water at both room temperature and 90 °C in sealed PTFE vessels. The leaching experiments were based on an accelerated leaching method ASTM C1308-08, which provides a procedure for measuring the leaching rates of elements from solid samples (ASTM-C1308-08, 2009). Leachates were exchanged at a 1-day interval with the sample surface-area-to-volume ratio (S/V) kept at 5.0 throughout the experiment for both composite and core-shell pellets. After the 14-day leaching experiment, Cs, Bi, and I concentrations in the leachates were analyzed using inductively coupled plasma mass spectrometry (ICP-MS; Varian 820). The corresponding leaching rate m(i) (mg m^{-2} d^{-1}) was calculated as follows (1):

$$m(i) = \frac{C_i V}{St} \quad (1)$$

where C_i is the concentration measured by an ICP-MS (mg L^{-1}), V is the

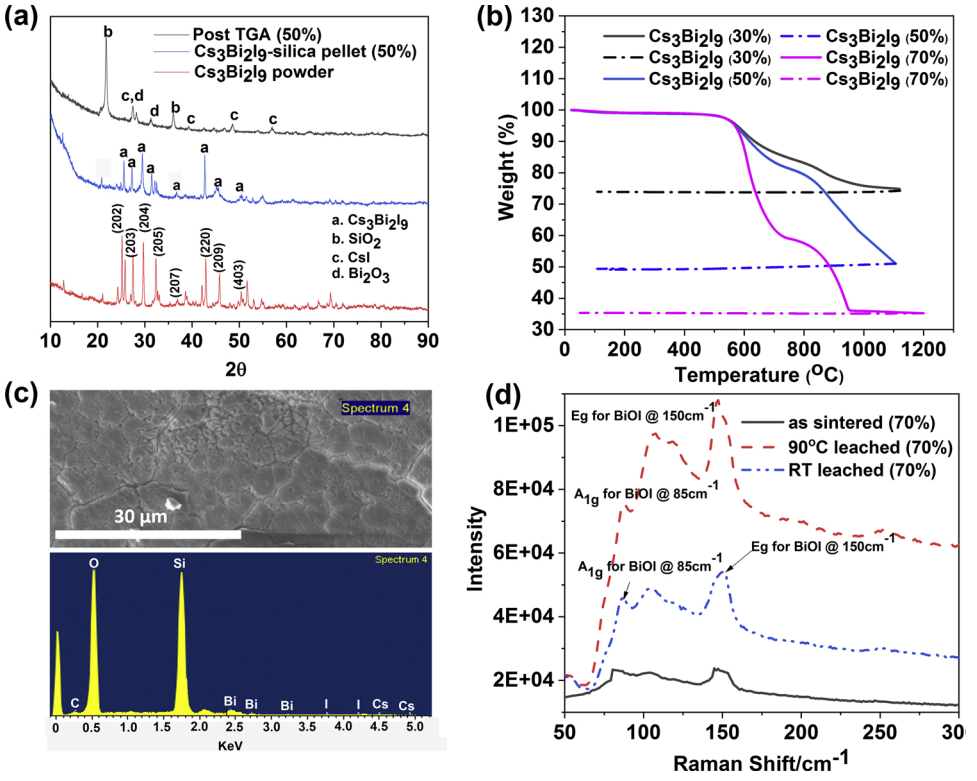

Fig. 2. XRD spectra (a) and TGA results (b) of the $Cs_3Bi_2I_9$-silica composites with different $Cs_3Bi_2I_9$ (wt.%) amounts (solid lines on heating, dashed lines on cooling); (c) An EDS spectrum of the 50 wt% $Cs_3Bi_2I_{9\text{-silica}}$ composite after thermal treatment at 1100 °C showing phase decomposition and loss of iodine and Cs; and (d) Raman spectra of the 70 wt.% composite before and post leaching tests in deionized water for 14 days (14-d) at room temperature and 90 °C.

leachate volume (L), S is the surface area of the coupon (m^2), and t is the sampling time interval (1 d). The S/V was maintained at 5.0 m^{-1} during the leaching experiment.

The long-term leaching rate (mg m^{-2} d^{-1}) can be evaluated based on a Cote's model (Cote et al., 1987), which is shown in Eq. (2):

$$m(t) = k_1 t + k_2 t^{1/2} + k_3(1 - e^{-k_4 t}) \quad (2)$$

Specifically, $m(t)$ stands for the cumulative leaching extent as mg m^{-2}, and the first term, $k_1 t$, represents a linear dissolution behavior. The second ($k_2 t^{1/2}$) and third [$k_3(1\text{-}e^{-k4t})$] terms are related to mass transport controlled by diffusion and species exchanging between the matrix surface and solution, respectively (Cote et al., 1987). Taking the derivative of the Cote's model with respect to time, the long-term dissolution rate can be derived based on the parameter k_1 assuming the leaching time approaching infinity.

3. Results and discussion

3.1. Microstructure, phase and composition of the SPS-sintered composites

The surface microstructures of the as-sintered $Cs_3Bi_2I_9$-silica composites with varied $Cs_3Bi_2I_9$ amounts are shown in Fig. 1. The highly densified composite pellets contain dual phases with dense silica particles surrounded by the $Cs_3Bi_2I_9$ grains, as shown by the different contrasts under SEM. The theoretical densities of the as-sintered composite pellets were measured as 90.5 %, 92 %, and 93.5 %, corresponding to 30, 50, and 70 wt.% of $Cs_3Bi_2I_9$, respectively. As the $Cs_3Bi_2I_9$ amount was increased from 30 to 70 wt.%, the interface between $Cs_3Bi_2I_9$ and silica particles was less obvious, because most of the pellet was composed of $Cs_3Bi_2I_9$ (Fig. 1). EDS measurements confirm the coexistence of $Cs_3Bi_2I_9$ and dense silica particles (Fig. 1d).

The TGA data shown in Fig. 2b suggests that the thermal decomposition of $Cs_3Bi_2I_9$ occurs at an onset temperature of 600 °C from 30 wt.% to 70 wt.% $Cs_3Bi_2I_9$. The mass loss monitored during the heating and cooling processes indicated that almost all the volatile elements of the $Cs_3Bi_2I_9$ incorporated into the composite structure was lost at the maximum heating temperature of 1100 °C, with only a small portion of mass loss occurring during the cooling procedure. The weight loss further confirmed that the perovskite $Cs_3Bi_2I_9$ was not decomposed during the SPS consolidation, and no appreciable loss of highly volatile iodine and Cs occurred during the SPS consolidation process.

XRD spectra of $Cs_3Bi_2I_9$ powders and as-sintered composite pellets (Fig. 2a) indicate a pure defect perovskite $Cs_3Bi_2I_9$ phase. In addition, no crystalline SiO_x phases were identified from XRD patterns of the composite, suggesting that the $Cs_3Bi_2I_9$ phase is encapsulated into an amorphous silica matrix since amorphous silica used herein cannot be crystallized at such a low SPS consolidation temperature. However, the XRD pattern of the composite pellet (50 wt.%) after 1100 °C TGA treatment displays minor CsI and Bi_2O_3 peaks as a result of phase decomposition and a possible reaction between bismuth with silica. Diffraction peaks of crystalline SiO_2 were also observed which might be indexed as cristobalite (ICSD01-076-0941) after 1100 °C TGA testing, suggesting that the amorphous silica matrix has been partially crystallized at a higher temperature. The EDS spectrum in Fig. 2c further confirms the retention of Cs, Bi, and I in the composite structure matrix after thermal treatment at 1100 °C. Fig. 2d shows Raman spectra of the composite (70 wt.% $Cs_3Bi_2I_9$) after sintering and the 14-d leaching test in aqueous solutions. Raman peak shifts were observed at 85 and 150

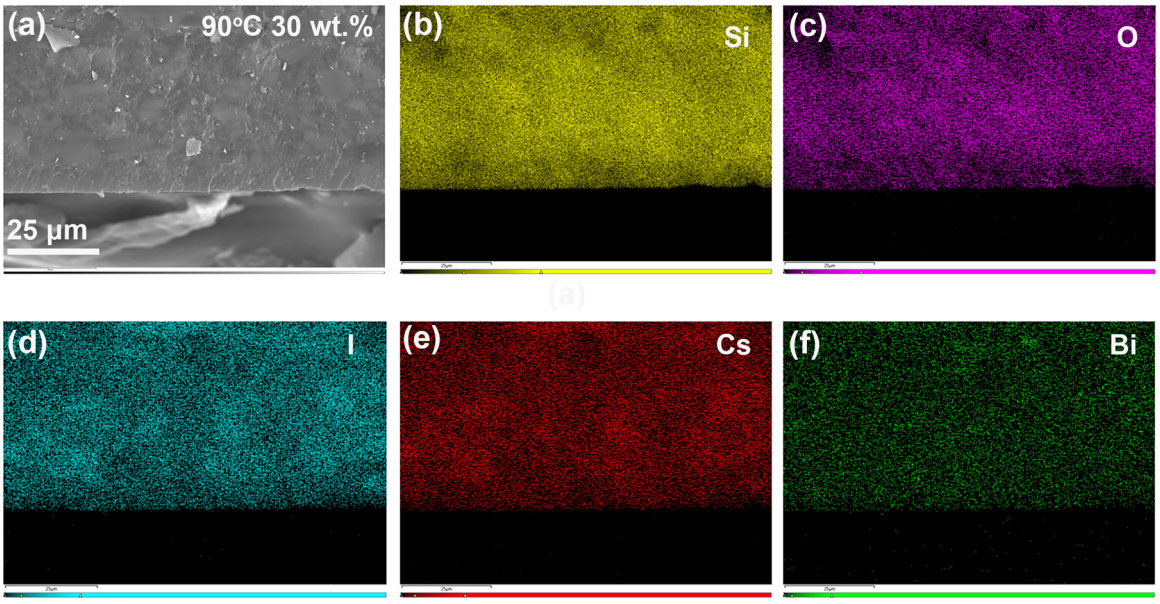

Fig. 3. A cross-sectional SEM image and the EDS elemental mappings of the 30 wt% $Cs_3Bi_2I_9$-silica composite after leaching in deionized water for 14 days at 90 °C. No obvious surface alteration and microchemistry evolution are observed across the top of the pellet surface towards the inner matrix.

cm^{-1}, corresponding to the A_{1g} and E_g Bi–I stretching modes of a BiOI phase for the samples leached at both RT and 90 °C. These results indicate that a secondary phase of BiOI formed by the interaction with water molecule (Fig. 2d) (Davies, 1973; Fan et al., 2016).

3.2. Microstructure and microchemistry evolution of the $Cs_3Bi_2I_9$-silica composites after semi-dynamic leaching

To understand the leaching behavior and chemical durability of the $Cs_3Bi_2I_9$-silica composites, a semi-dynamic leaching experiment of the composites was carried out for 14 days at room temperature and 90 °C. The SEM and EDS mapping were performed to investigate the morphology, microstructure, and microchemistry variations across the leached samples. Figs. 3–5 show the cross-sectional elemental mappings of the composite pellets after leaching for 14 days at room temperature or 90 °C. No obvious morphology and microstructure evolution can be observed in the 30 wt.% composite pellet post the 14-d leaching (Fig. 3). The corresponding element mappings suggest that no significant variation of the microchemistry across from the top surface to the center of the pellets occurs for the 30 wt.% composite pellet at 90 °C

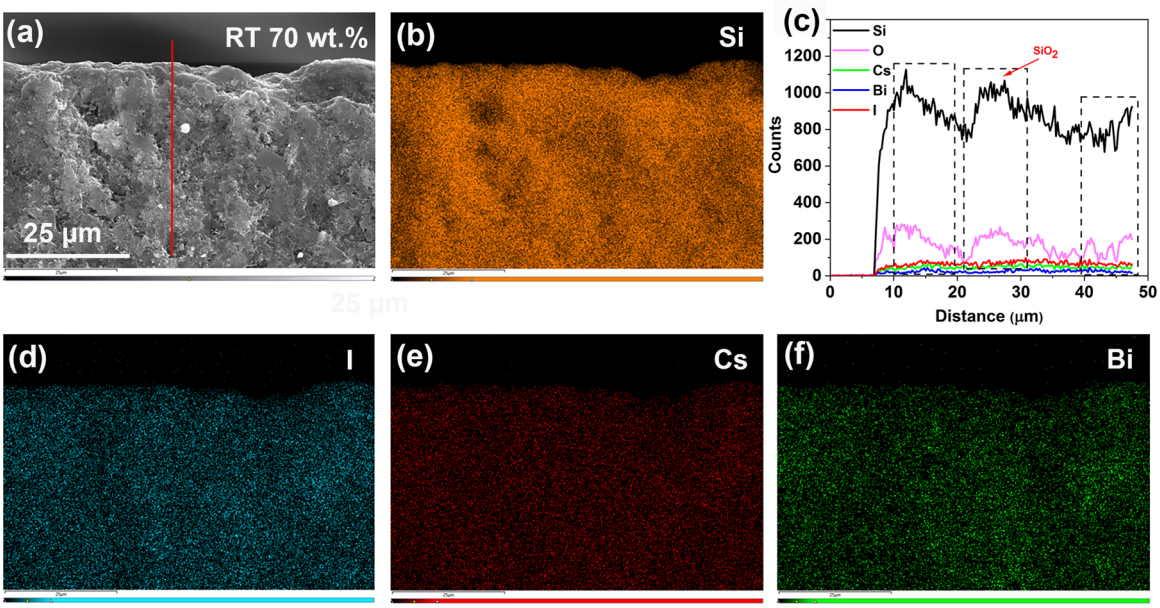

Fig. 4. A cross-sectional SEM image and the EDS elemental mappings of the 70 wt% $Cs_3Bi_2I_9$-silica composite after leaching in deionized water for 14 days at room temperature. No obvious surface alteration and morphology evolution are observed. An EDS line scan (c) shows elemental variations though silica matrix.

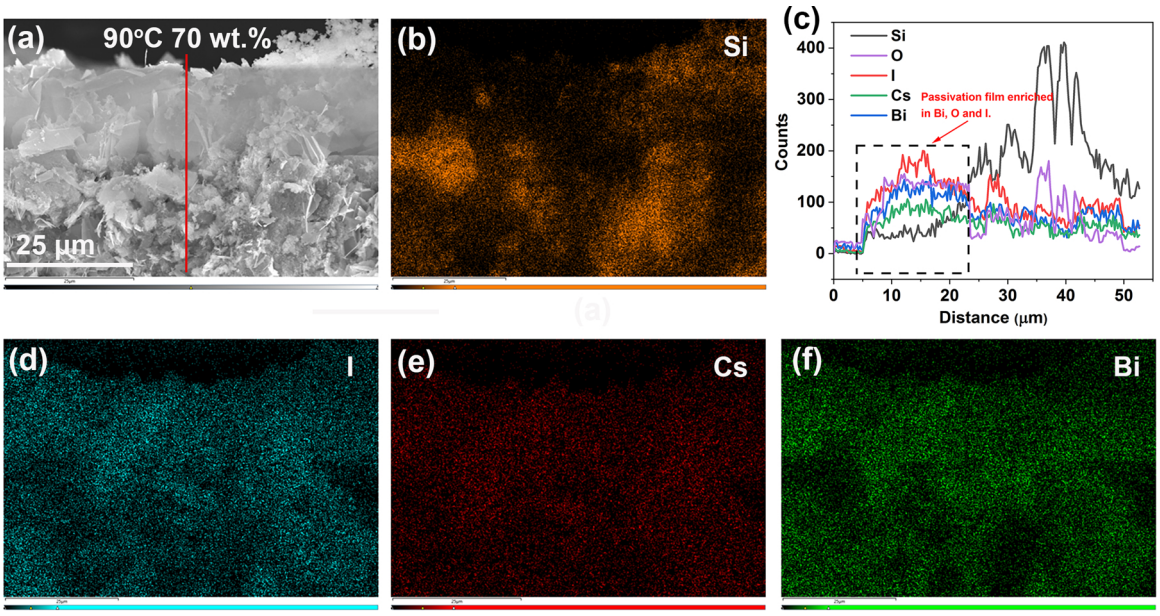

Fig. 5. A cross-sectional SEM image and the EDS elemental mapping of the $Cs_3Bi_2I_9$-silica (70 wt.%) after leaching in deionized water for 14 days at 90 °C. A 15 μm-thick surface alteration layer formed with the formation of BiOI nanosheets. An EDS line scan (c) from the top surface to the inner matrix in the SEM image showing the enrichment of Bi, O and I in the alteration layer as compared with the matrix.

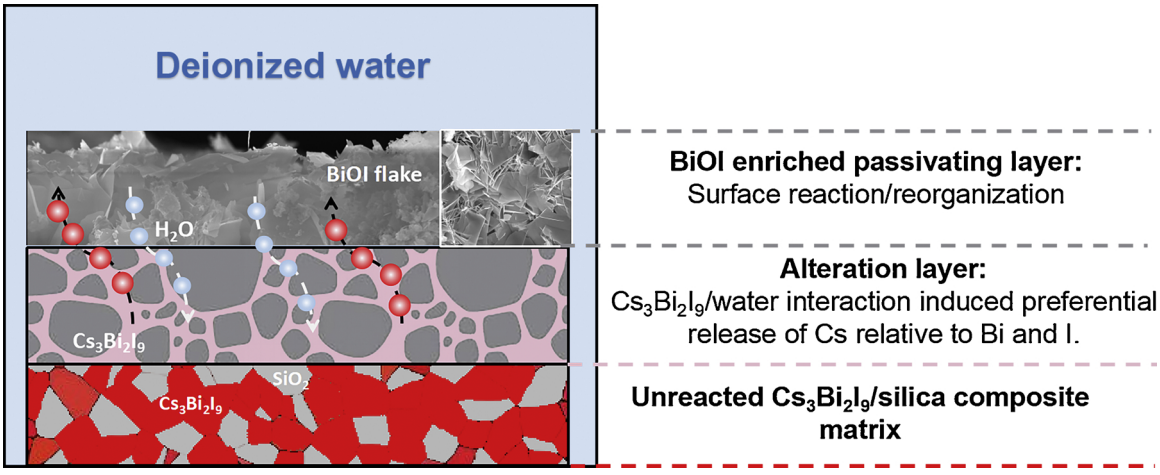

Fig. 6. A representative scheme to illustrate the surface alteration process of the $Cs_3Bi_2I_9$/silica composite in deionized water containing multiple steps processes of dissolution, diffusion and reorganization.

(Fig. 3), and the 70 wt.% composite (Fig. 4) leached at room temperature for 14 days.

Compared with the room temperature leaching test (Fig. 4), the cross-section SEM image (Fig. 5a) of the 70 wt.% composite sample leached at 90 °C for 14 days in deionized water shows a flake-like nanosheet alteration layer of approximately 15-μm underneath the top surface of the pellet. Both the EDS elemental mappings and the line-scan data as shown Fig. 5 indicated that the alteration layer was enriched in Cs, Bi, O, and I, but depleted in Si. Specifically, Bi, O, and I concentrations were higher in the alteration layer as compared with the matrix underneath. The Cs concentration was also found to be slightly higher in the alteration layer than in the matrix. The alteration layer is consistent with the Raman spectra shown in Fig. 2d showing distinct active Raman modes from a layered BiOI, identical to the results reported previously (Fan et al., 2016). The formation of the BiOI results from a chemical reaction between BiI_3 and water: $BiI_3(S) + H_2O \rightarrow BiOI(S) + 2HI(aq)$ when Cs^+ is released out from the perovskite crystals (Fan et al., 2016). The observation of more BiOI formed on the sample surface at 90 °C than the sample at room temperature demonstrates that the chemical reaction is endothermic with

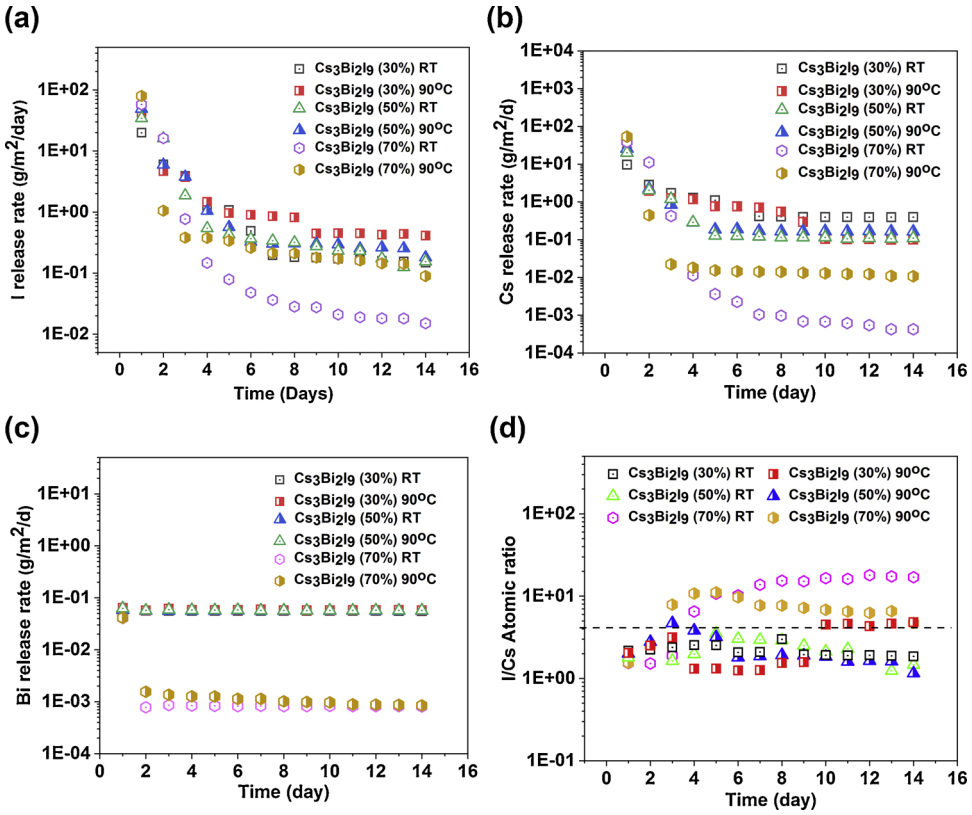

Fig. 7. Elemental release rates of I (a), Cs (b), and Bi (c) for the composites with different $Cs_3Bi_2I_9$ amounts in a semi-dynamic leaching testing in deionized water at room temperature and 90 °C, and the atomic ratio of I:Cs in bulk solutions as measured by ICP-MS (d).

increased reaction kinetic at higher temperatures. No obvious alteration was observed in the 30 and 50 wt.% $Cs_3Bi_2I_9$-contained composites. This comparison indicates that the formation of BiOI could be attributed to enhanced chemical reactions and accelerated element release from the composite with greater amounts of $Cs_3Bi_2I_9$ and higher temperatures. Details of the surface alteration mechanism will be illustrated in Section 3.3 and Fig. 6.

3.3. Chemical durability and leaching mechanisms of $C_3Bi_2I_9$–silica composites

The time evolution of the elemental release rates from the perovskite-silicate composites into the leachate is shown in Fig. 7. The initial release rates for first few days were significantly higher for Cs, Bi, and I. The elemental release rates decreased gradually before reaching a long-term steady state. The measured accumulative concentrations of I,

Table 1
Long term release rates and normalized long term rates of Cs, Bi and I calculated by the Cote's Model for composites and core-shell structure.

Long-term rate	30 wt.%		50 wt.%		70 wt.%		20 wt.% core–shell	
($g/m^2/d$)	RT	90 °C	RT	90 °C	RT	90°C	RT	90 °C
I	0.140	0.380	0.150	0.100	0.011	0.025	3.12E-06	5.00E-06
Cs	0.110	0.100	0.089	0.09	4E-4	0.004	5.00E-06	9.70E-05
Bi	0.0556	0.053	0.056	0.055	6.16E-04	4.83E-04	1.03E-06	1.40E-06
N-Long-term rate	30 wt.%		50 wt.%		70 wt.%		20 wt.% core–shell	
($g_N/m^2/d$)	RT	90 °C	RT	90 °C	RT	90°C	RT	90 °C
I	0.778	2.111	0.500	0.333	0.026	0.059	3E-5	4E-5
Cs	1.8333	1.667	0.890	0.9 00	0.003	0.032	0.00013	0.0024
Bi	0.927	0.883	0.560	0.550	0.004	0.004	3E-5	4E-5

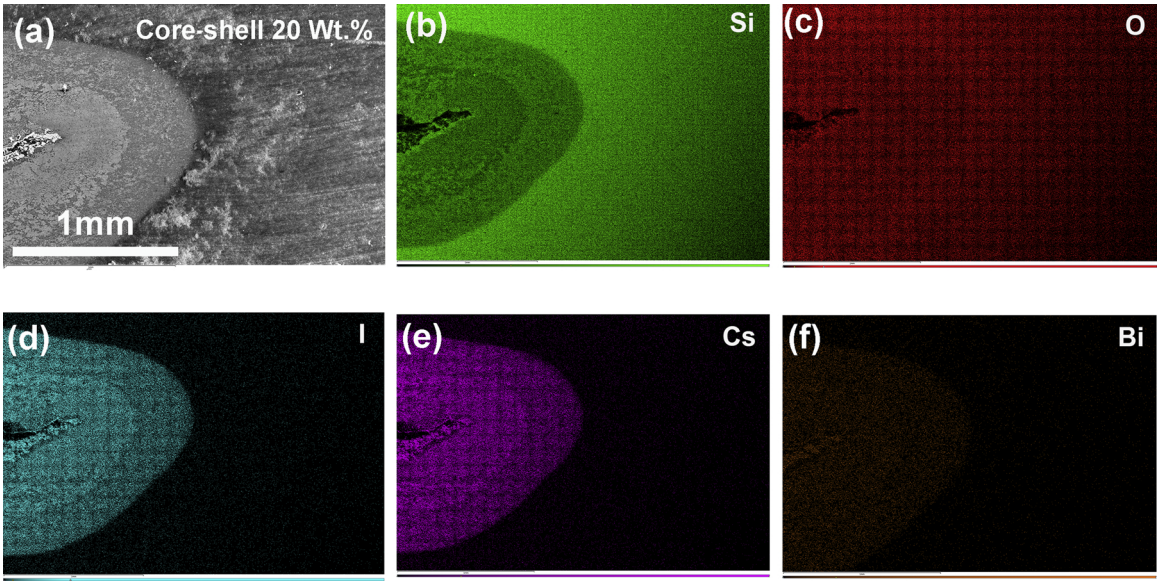

Fig. 8. SEM micrograph and EDS elemental mappings showing microstructure and elemental distribution in the 20 wt.% $Cs_3Bi_2I_9$–silica core–shell structure.

Cs, and Bi (shown in Fig. S2- Supplemental Materials) in bulk solutions were fitted by the Cote's model shown in Eq. (2), and the corresponding parameters are shown in Tables S1–3. The long-term leaching rates can be derived from the value k_1 in the fitting curves, as summarized in Table 1. Surprisingly, the long-term rates were higher for the 30 wt.% $Cs_3Bi_2I_9$-silica compositefollowed by 50 wt.% $Cs_3Bi_2I_{9\text{-silica}}$composite. The 70 wt.% $Cs_3Bi_2I_9$-silica composite displays the lowest element release rate despite that the overall elemental accumulated concentrations in bulk solutions are the highest (Fig. S2- Supplemental Materials).

The lowest long-term elemental release rate for the 70 wt.% $Cs_3Bi_2I_9$-silica composite can be attributed to the rapid formation of a protective BiOI layer for the sample pellet with higher amounts of $Cs_3Bi_2I_9$ loading and higher leachate temperatures. This phenomenon is consistent with the observation of the BiOI passive film formation as evidenced by Raman, and EDS elemental mapping data (shown in Figs. 2d and 5). Detailed surface alteration phenomena can be illustrated in the schematic Fig. 6, which follows a dissolution-diffusion-reorganization process. Specifically, because of higher concentration of $Cs_3Bi_2I_9$ in the 70 wt.% compsites, initial Cs and I release rates are expected higher (as evidenced in Fig. 7a and b) and the elemental release follows a dissolution-controlled mechanism at the initial leaching stage within 2–3 days. The rapid release of Cs and I at the initial stage for the 70 wt.% $Cs_3Bi_2I_9$ at 90 °C results in a hydrated surface layer containing both BiI_3, CsI and H_2O molecules. Surface reaction/reorganization between BiI_3/water may occur, resulting in an flake-like BiOI enriched passivating layer on the surface as shown in Fig. 6. For the 30 wt.% and 50 wt.% composite pellets, $Cs_3Bi_2I_9$ crystals were segregated and separated by the silica gel particles as indicated in the SEM images (Fig. 1a and b), which may slow down the formation of the BiOI protective layer. Therefore, with the rapid formation of a passive BiOI layer in preventing further element release from the matrix with 70 wt.% $Cs_3Bi_2I_9$, the long-term release rates of Cs, Bi, and I decrease accordingly with increased $Cs_3Bi_2I_9$ amount from 30 wt.% to 70 wt.%, which makes the $Cs_3Bi_2I_9$-silica composite structure an ideal waste form for immobilization of Cs and I.

Fig. 7d shows the atomic ratios of I:Cs of different composites leached into bulk solutions at room temperature and 90 °C, which may provide valuable information on the dissolution mechanisms. For all samples, the I:Cs atomic ratios with respect to time were composed of two distinct stages. The initial I:Cs atomic ratios within the first 3 days are lower than the stoichiometric ratios of 3.0, suggesting a non-congruent dissolution and more rapid release of Cs from the perovskite that was higher than iodine. The rapid release of Cs can be attributed to the structural characteristics of the defect perovskite derivation $Cs_3Bi_2I_9$. Specifically, $Cs_3Bi_2I_9$ crystallizes into a layered crystal structure with the $(Bi_2I_9)^{3-}$ forming as a pair of face-sharing BiI_6 octahedra, resulting in a hexagonal layered structure with the Cs atoms filling the hexagonal channels between layers (Aleksandrov and Beznosikov, 1997). Therefore, the weak bonds between the layer structure can be broken easily, leading to the rapid release of Cs^+. The preferential release of weakly-bonded cations results in a non-congruent dissolution behavior, like what observed in glass waste forms (Weissbart and Rimstidt, 2000). After the initial rapid release of I and Cs, the I:Cs atomic ratios for all six composite samples either reached a constant stage or showed a decrease. This can be explained by the surface reorganization to produce a water-insoluble BiOI passivating layer after the preferential release of Cs and the reaction of the 2D BiI_3 with water. The formation of the BiOI passivating layer may slow down the release of iodine, decreasing the I:Cs ratios continuously in bulk solutions (Krumhansl and Nenoff, 2011).

3.4. $Cs_3Bi_2I_9$-silica core–shell structure

In order to further improve the corrosion resistance and reduce the release rate of the major elements from the waste form matrix, a $Cs_3Bi_2I_9$-silica core-shell structure with maximum $Cs_3Bi_2I_9$ loading of 20 wt.% was fabricated, in which the perovskite with high loadings of Cs and I was fully encapsulated into a silica matrix. The core-shell structure was previously reported for a lead iodoapatite waste form with an

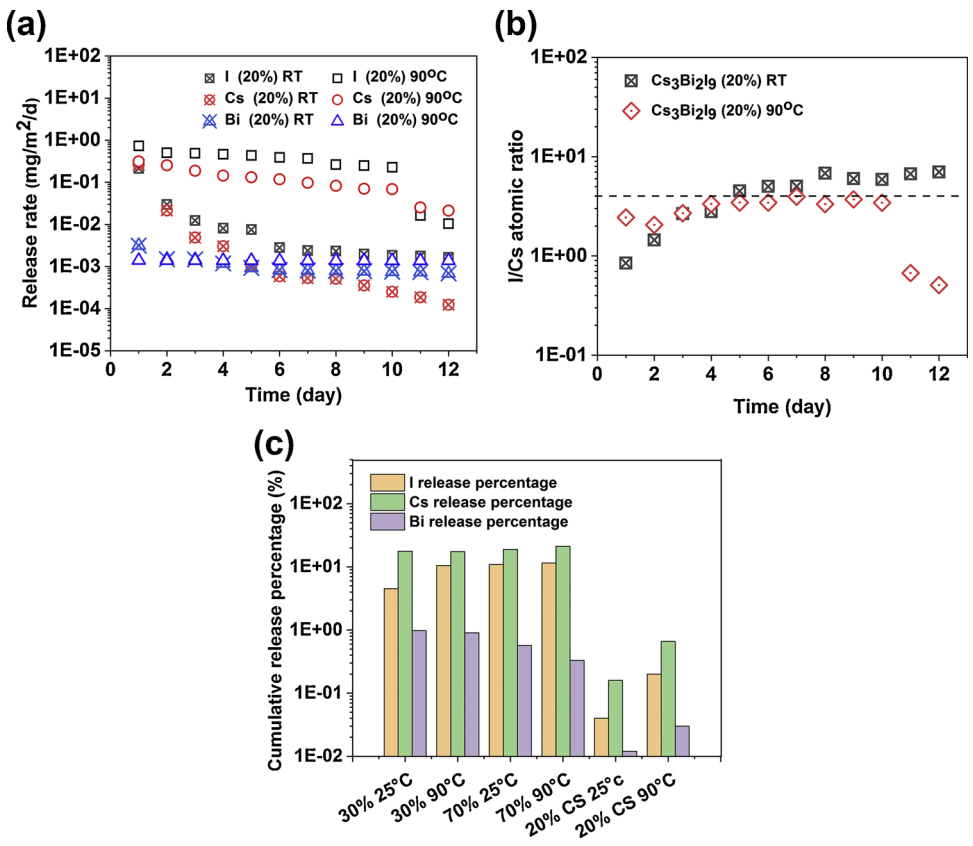

Fig. 9. Elemental release rates (a) of Cs, Bi, and I of the 20 wt.% $Cs_3Bi_2I_9$-silica core-shell structure, and the I:Cs atomic ratio (b) in a semi-dynamic leaching testing in deionized water at room temperature and 90 °C; and (c) Elemental release percentages for the composite (14 days) and core-shell structures (12 days) in deionized water at room temperature and 90 °C.

Table 2
Summary of various Cs and I immobilization methods and the corresponding leaching conditions.

Materials	Leaching Method	leachate	Temp. (°C)	S/V (m^{-1})	Reference
Glassified sodalite (I)	ASTM C1308	DIW	90	8	Chong et al., 2018
Iodate-incorporated hydroxyapatite	MCC-1	DIW	90	4.6	Campayo et al., 2011
Apatite: lead vanadate (PbV) (I)	MCC-1	DIW	90	0.8	Guy et al., 2002
Silver phosphate glass (I)	PCT-A(C1285)	DIW	90	2000	Yang et al., 2017
Silver iodate sodalite (I)	MCC-1	DIW	90	10	Maddrell et al., 2019
Lead iodoapatite (I)	MCC-5	DIW	90	0.1	Uno et al., 2001
$(3M_2O)(3Al_2O_3)(6SiO_2)(2MX)$ (I)	MCC-5	DIW	100	0.1	Babad and Strachan,1980
$PbO\text{-}B_2O_3$-based glass (I)	undefined Test	0.55 M NaCl	RT	10	Tanabe et al., 2010
Magnesium potassium phosphate matrices (I)	ANS 16-1	DIW	RT	1	Vinokurov et al., 2009
Ag-exchanged mordenite(HIP 17-8) (I)	ASTM C1220-10	DIW	90	10	Lawter et al., 2019
Ag-functionalized silica aerogels (I)	ASTM C1662-17	Buffer, pH = 11	90	10	Asmussen et al., 2019
$(Ba,Cs)(Al,Ti)_2Ti_6O_{16}$ (Cs)	MCC-1	DIW	90	10	Carter et al., 2002
Hollandite ($BaCs_{0.28}Fe_{0.82}Al_{1.46}Ti_{5.72}O_{16}$)	MCC-1	DIW	90	10	Angeli et al., 2008
Borosilicate (Cs)	MCC-1	DIW	90	10	Lee et al., 2013
Portland cement (Cs)	GOST 29114-91	DIW	RT	8.6	Ojovan et al., 2011
Struvitec (CsCl)-borosilciate matrix	ANS 16-1	DIW	RT	1	Wagh et al., 2016
Cs-pollucite + SiO_2 (Cs)	MCC-5	DIW	97	0.1	Yanagisawa et al., 1987
HIPed tailored hollandite (Cs)	MCC-1	DIW	90	10	Carter et al., 2009
$Cs_{0.21}Na_{0.12}W_{0.07}Mo_{0.02}O_3$ (Cs)	MCC-1	DIW	150	10	Luca et al., 2004
$Ba_{0.85}Cs_{0.26}Al_{1.35}Fe_{0.77}Ti_{5.9}O_{16}$ (Cs)	UndefinedTest	pH = 8.4	95	5000	Muresan et al., 2011
$Cs_3Bi_2I_9$-silica composite (70 wt.%)	ASTM C1308	DIW	90	5	Study herein
$Cs_3Bi_2I_9$-silica core–shell (20 wt.%)	ASTM C1308	DIW	90	5	Study herein

Table 3
Summary of various Cs and I immobilization capacity and corresponding normalized long-term rates.

Materials	Immobilization capacity (mass%)	Normalized rate (mg/m^2/d)	Reference
Glassified sodalite (I)	9.3	1290	Chong et al., 2018
iodate-incorporated hydroxyapatite	7	1.429	Campayo et al., 2011
Apatite: lead vanadate (PbV) (I)	8.6	27.91	Guy et al., 2002
Silver phosphate glass (I)	17	0.17	Yang et al., 2017
Silver iodate sodalite (I)	15	16	Maddrell et al., 2019
Lead iodoapatite (I)	7.2	5527.78	Uno et al., 2001
$(3M_2O)(3Al_2O_3)(6SiO_2)(2MX)$ (I)	12.7	70,000	Babad and Strachan, 1980
$PbO\text{-}B_2O_3$-based glass (I)	1.7	500	Tanabe et al., 2010
Magnesium potassium phosphate matrices (I)	4	1120	Vinokurov et al., 2009
Ag-exchanged mordenite(HIP 17-8)(I)	3	18	Lawter et al., 2019
Ag-functionalized silica aerogels(I)	24.9	23	Asmussen et al., 2019
$(Ba,Cs)(Al,Ti)_2Ti_6O_{16}$ (Cs)	1.66	5	Carter et al., 2002
Hollandite ($BaCs_{0.28}Fe_{0.82}Al_{1.46}Ti_{5.72}O_{16}$)(Cs)	0.96	5	Angeli et al., 2008
Borosilicate (Cs)	10	30	Lee et al., 2013
Portland cement (Cs)	1.6	700	Ojovan et al., 2011
Struvitec (CsCl)-borosilciate matrix	1.58	266	Wagh et al., 2016
Cs-pollucite + SiO_2 (Cs)	0.49	3150	Yanagisawa et al., 1987
HIPed tailored hollandite (Cs)	6	69	Carter et al., 2009
$Cs_{0.21}Na_{0.12}W_{0.07}Mo_{0.02}O_3$ (Cs)	10	7	Luca et al., 2004
$Ba_{0.85}Cs_{0.26}Al_{1.35}Fe_{0.77}Ti_{5.9}O_{16}$	0.92	0.08	Muresan et al., 2011
$Cs_3Bi_2I_9$-silica composite (70 wt.%)	42(I), 14(Cs)	59.5(I),31.8(Cs)	Study herein
$Cs_3Bi_2I_9$-silica core–shell (20 wt.%)	12(I), 4(Cs)	0.008(I),2.4(Cs)	Study herein

iodine-free vanadate shell that can significantly improve the chemical durability of the waste form matrix (Guy et al., 2002). However, less than 5 wt.% iodine was incorporated into the lead iodoapatite waste form due to the low iodine content and higher material density in the iodoapatite host phase (Guy et al., 2002). In comparison, the cross-sectional microstructure of as-sintered core-shell structure with 20 wt.% $Cs_3Bi_2I_9$ is shown in Fig. 8 along with the corresponding elemental distribution EDS mappings. The cross-section SEM image indicates a sandwich structure with a light color core of $Cs_3Bi_2I_9$ and a darkly-colored silica shell corresponding to the optical images inset in Fig. 8a with a red colored core of $Cs_3Bi_2I_9$ embedded in a dense silica glass matrix. The corresponding EDS mappings demonstrate the successful encapsulation of $Cs_3Bi_2I_9$ into the silica shell without any Cs, Bi, and I release out from the core-shell structure. Despite minor phase decomposition and migration of the Cs and I through the matrix leading to a 200-μm diffusion ring with progressively less Cs and I than the inner core, a sharp interface can be observed in the elemental distribution of Cs and I (Fig. 8d and e). This implies that all the Cs and I are confined into the core-shell structure without escaping from the silica matrix. A similar observation was reported previously for a Cs_2SnCl_6/lead apatite core-shell structure fabricated by Scott (2017).

The silica shell behaves as an effective barrier layer to prevent water transport and corrosion of the $Cs_3Bi_2I_9$ core. In composites, micrometer-sized $Cs_3Bi_2I_9$ crystals are embedded into a silica matrix, and a dual-phase structure in a composite geometry formed. Therefore, the core-shell structure is expected to display greatly-enhanced radionuclide immobilizing ability compared to the composite structure which can be confirmed by chemical dissolution experiments. Fig. 9a and b show the elemental leaching rates and I:Cs atomic ratio from the core-shell structure with 20 wt.% perovskite after exposed to aqueous solutions for 12 days at room temperature and 90 °C. The corresponding Cs, Bi, and I release rates are orders of magnitude lower compared to composite structures for both room temperature and 90 °C corresponding to its physical structure. The leaching rates gradually decreased from day-1 to day-12 for all of the three elements of Cs, Bi and I (Fig. 9a) without a rapid decreasing trend as compared to the composite structure due to an excellent barrier effect of the dense silica shell.

The atomic ratio of I:Cs also gradually increased with the breaking of Cs–I bonds and reached the congruent stage with I:Cs approaching to 3.0 for room-temperature leaching tests. However, the initial congruent

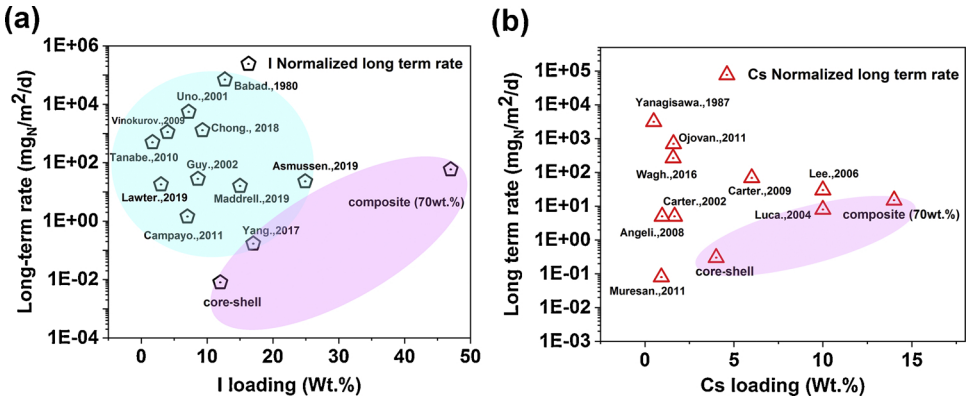

Fig. 10. Chemical durability and waste loading metric of the composite and core-shell structures in comparing with the state-of-the-art results among different leading waste form materials for I (a) and Cs (b). The chemical durability is evaluated by the corresponding normalized long-term release rate. This comparison shows simultaneously-enhanced chemical durability and waste loadings for the $Cs_3Bi_2I_9$-based composites and core-shell structure.

release of Cs and I shift to incongruent with I:Cs significantly lower than 3.0 after 9-d leaching for the core-shell sample at 90 °C, which can be attributed to the gradual formation of water-insoluble BiOI at 90 °C similar to composite structure (Fig. 9b). The maximum release rates determined after the first day are 0.850 mg m^{-2} d^{-1} for iodine, 0.300 mg m^{-2} d^{-1} for Cs, and 0.030 mg m^{-2} d^{-1} for Bi at 90 °C, respectively. Fig. 9c compares the accumulative Cs, Bi, and I release percentages for the composite samples and the core-shell structure. The total I and Cs release percentages are 0.18 % and 0.49 % for the 20 wt.% core-shell sample at 90 °C, an order of magnitude lower than those of the composite structure at the end of the experiment, indicating better chemical durability for the core-shell structure.

3.5. Chemical durability and waste loading as compared with literature

In this section, the $Cs_3Bi_2I_9$ perovskite-silica composite waste form and the core-shell structure are further compared with literature from the aspects of chemical durability and waste loadings, the key characteristics for waste form design and performance evaluation, which are summarized in Table 2 and 3 and Fig. 10. Fig. 10a compares the normalized long-term release rate of iodine and iodine loadings of the composite and core-shell structure in this study and leading iodine waste forms from literature including silver iodate sodalite, lead-vanadate iodoapatite, as well as others in the literature (Chong et al., 2018; Campayo et al., 2011; Angeli et al., 2008; Yang et al., 2017; Maddrell et al., 2019; Uno et al., 2001; Babad and Strachan, 1980; Wagh et al., 2016; Ojovan et al., 2011; Asmussen et al., 2019; U.S.E.P.A., 2012). The long term release rates are normalized with respect to the element contents for a direct comparison based on the equation (3), where R_N stands for the normalized long term rate (mg_N m^{-2} d^{-1}) and can be calculated by dividing the long term rate (R) with the element contents in the matrix (f_i):

$$R_N = \frac{R}{f_i} \tag{3}$$

In general, the normalized long-term release rate of iodine spans several orders magnitudes from highly soluble glassified sodalite to highly durable iodoapatite, and the waste loading is typically less than 10 wt.%. The 70 wt.% $Cs_3Bi_2I_9$-silica composite has iodine loading up to 42 wt.%, significantly higher than the highest I loading (24.9 wt.%) ever reported for Ag-functionalized silica aerogel (Asmussen et al., 2019). The normalized long-term release rate is comparable to the previous widely studied waste forms (Chong et al., 2018; Campayo et al., 2011; Angeli et al., 2008; Yang et al., 2017; Maddrell et al., 2019; Uno et al., 2001; Babad and Strachan, 1980; Wagh et al., 2016; Ojovan et al., 2011; Asmussen et al., 2019; U.S.E.P.A., 2012). On the other hand, the core-shell structure displays the best chemical durability among all the materials reported. The normalized long-term release rate of iodine for the core-shell structure is two orders of magnitude lower than that of iodine waste forms with the best performance reported in literature (specifically, silver phosphate glass) (Yang et al., 2017). The iodine waste loading of the core-shell structure is 12 wt.%, comparable to sodalite $(3M_2O)(3Al_2O_3)(6SiO_2)(2MX)(I)$ and much higher than the majority of waste forms listed in the Table 2 (Babad and Strachan, 1980). Along with the iodine, the waste forms studied herein can also immobilize Cs at the same time. A maximum of 14 wt.% of cesium can be incorporated in the composite structure, ranking the highest Cs loading among the waste forms listed in Tables 2 and 3. The normalized long-term rate of Cs for the 70 wt.% composite is relatively low with a comparable chemical durability to $Cs_{0.21}Na_{0.12}W_{0.07}Mo_{0.02}O_3$ (Luca et al., 2004). The core-shell structure containing 4 wt.% of Cs loading displays the second lowest Cs normalized release rate (2.400 mg_N m^{-2} d^{-1}) due to the unique microstructure and the durable silica shell greatly improving their chemical durability. $Ba_{0.85}Cs_{0.26}Al_{1.35}Fe_{0.77}Ti_{5.9}O_{16}$ matrix (Muresan et al., 2011) has a lower normalized long-term release rate but also significantly lower Cs loading (0.92 wt.%) than the core-shell structure reported here. These results clearly indicate that the composite and core-shell structure by effectively encapsulating iodine and Cs-bearing phases into a durable glass matrix will greatly improve chemical durability and meanwhile maintain very high waste loadings. Meanwhile, the low temperature-high pressure SPS consolidation technique provides a robust way to immobilize the highly volatile radioactive nuclides, including I and Cs, which might open up new materials and design strategies that can potentially be used to immobilize the highly mobile radionuclides. Compared with the state-of-the-art materials in the field (as shown in Table 2 and Fig. 10), the proposed composite and core-shell structures display great potentials as environmentally-benign waste forms for simultaneous immobilization of Cs and I with an optimized balance of excellent chemical durability and high waste loadings.

4. Summary and conclusions

In this work, we demonstrate viable waste forms for long-lived and problematic I-129 and Cs-135 with high waste loadings and exceptional chemical durability based on the combination of a defect perovskite $Cs_3Bi_2I_9$ and silica matrix in composite and core-shell structures. Composites with up to 70 wt.% defect perovskite can be fabricated by a low temperature SPS process. High chemical durability can be achieved by fully encapsulating the 20 wt.% of $Cs_3Bi_2I_9$ into the silica matrix to form a core-shell structure. Increasing the $Cs_3Bi_2I_9$ ratio in the composite results in a lower long-term release rate by accelerating the formation of a passivating BiOI layer through multiple bulk solid-liquid interface reactions. The main findings include the following:

- Amorphous silica matrix can act as a physical barrier at both micro-level and engineering-level to significantly slow down the $Cs_3Bi_2I_9$/water interaction and element diffusion for the composites and core-shell structure, significantly decreasing the element release rate and improving the chemical durability of the designed waste forms;
- Surface reaction and reorganization can occur on the surface alteration of the $Cs_3Bi_2I_9$-silica composite *via* initial fast dissolution-long term diffusion process, leading to the formation of a water-insoluble BiOI passivating layer on the solid/liquid interface at elevated temperatures;
- An incongruent leaching mechanism dominates the dissolution of $Cs_3Bi_2I_9$ silica waste forms and the formation of a passivating BiOI layer eventually controls the kinetics of element transport throughout the solid matrix to bulk solution;

As a result of excellent chemical durability and very high waste loadings, the defect perovskite $Cs_3Bi_2I_9$-silica composite and the core-shell structure are promising waste form materials for effective waste management. The perovskite-structural type may also show potentials as a candidate host phase to immobilize other halides, *e.g.*, F^- and Cl^- for managing complex waste streams from advanced nuclear energy systems such as molten salt reactors and advanced chemical processing of used fuels.

CRediT authorship contribution statement

Kun Yang: Data curation, Writing - original draft. **Weiguang Zhu:** Data curation. **Spencer Scott:** Methodology. **Yachun Wang:** Methodology. **Jianwei Wang:** Writing - review & editing. **Brian J.**

Riley: Writing - review & editing. **John Vienna:** Writing - review & editing. **Jie Lian:** Supervision, Conceptualization, Methodology, Funding acquisition, Writing - review & editing.

Acknowledgment

This work was supported as part of the Center for Performance and Design of Nuclear Waste Forms and Containers (WastePD), an Energy Frontier Research Center (EFRC) funded by the U.S. Department of Energy, Office of Science, Basic Energy Sciences under Award DE-SC0016584. We also acknowledge the help from the manager of Microanalytical Laboratory, Jared W. Singer, for discussion of ICP-MS experimental data acquisition and analysis. Pacific Northwest National Laboratory is operated by Battelle Memorial Institute for the DOE under contract DE-AC05-76RL01830.

Appendix A. Supplementary data

Supplementary material related to this article can be found, in the online version, at doi:https://doi.org/10.1016/j.jhazmat.2020.123279.

References

Aleksandrov, K.S., Beznosikov, V.V., 1997. Hierarchies of pervoskite-like crystals (Review). Phys. Solid State 39 (5), 695–715. https://doi.org/10.1134/1.1130120.

Ambashta, R.D., Sillanpaa, M.E.T., 2012. Membrane purification in radioactive waste management: a short review. J. Environ. Radioact. 105, 76–84. https://doi.org/10.1016/j.jenvrad.2011.12.002.

Amoroso, J., Marra, J., Conradson, S.D., Tang, M., Brinkman, K., 2014. Melt processed single phase hollandite waste forms for nuclear waste immobilization: $Ba_{1.0}Cs_{0.3}A_{2.3}Ti_{5.7}O_{16}$; A = Cr,Fe,Al. J. Alloys. Compd. 584, 590–599. https://doi.org/10.1016/j.jallcom.2013.09.087.

Angeli, F., McGlinn, P., Frugier, P., 2008. Chemical durability of hollandite ceramic for conditioning cesium. J. Nucl. Mater. 380, 59–69. https://doi.org/10.1016/j.jnucmat.2008.07.003.

Asmussen, R.M., Ryan, J.V., Matyas, J., Crum, J.V., Reiser, J.T., Avalos, N., McEiroy, E.M., Lawter, A.R., Canfield, N.C., 2019. Investigating the durability of iodine waste forms in dilute conditions. Materials 12 (686), 1–22. https://doi.org/10.3390/ma12050686.

ASTM-C1308-08, 2009. Accelerated Leach Test for Diffusive Releases From Solid Waste and a Computer Program to Model Diffusive, Fractional Leaching From Cylindrical Waste Forms. ASTM International, West Conshohocken, PA.

Babad H., Strachan D.M. 1980. Method for immobilizing radioactive iodine. U.S Patent No.: 4229317.Available:https://patentimages.storage.googleapis.com/38/aa/e9/d8dddce59bc6cb/US4229317.pdf.

Brown, C.F., Geiszler, K.N., Lindberg, M.J., 2007. Analysis of 129I in groundwater samples: direct and quantitative results below the drinking water standard. Appl. Geochem. 22, 648–655. https://doi.org/10.1016/j.apgeochem.2006.12.010.

Campayo, L., Grandjean, A., Coulon, A., Delorme, R., Vantelon, D., Laurencin, D., 2011. Incorporation of iodates into hydroxyapatites: a new approach for the confinement of radioactive iodine. J. Mater. Chem. 21, 17609–17611. https://doi.org/10.1039/C1JM14157K.

Carter, M.L., Vance, E.R., Mitchell, D.R.G., Hanna, J.V., Zhang, Z., Loi, E., 2002. Fabrication, characterization and leach testing of hollandite, $(Ba,Cs)(Al,Ti)_2Ti_6O_{16}$. J. Mater. Res. 17 (10), 2578–2589. https://doi.org/10.1557/JMR.2002.0374.

Carter, M.L., Gillen, A.L., Olufson, K., Vance, E.R., 2009. HIPed tailored hollandite waste forms for the immobilization of radioactive Cs and Sr. J. Am. Ceram. Soc. 92 (5), 1112–1117. https://doi.org/10.1111/j.1551-2916.2009.03021.x.

Chong, S.H., Peterson, J.A., Riley, B.J., Tabada, D., Wall, D., Corkhill, C.L., McCloy, J.S., 2018. Glass bonded iodosodalite waste form for immobilization of ^{129}I. J. Nucl. Mater. 504, 109–121. https://doi.org/10.1016/j.jnucmat.2018.03.033.

Cote, P.L., Constable, T.W., Moreira, A.J.N., 1987. An evaluation of cement-based waste forms using the results of approximately two years of dynamic leaching. Nucl. Chem. Waste Manag. 7 (2), 129–139. https://doi.org/10.1016/0191-815X(87)90007-6.

Davies, J.E.D., 1973. Solid state vibrational spectroscopy-III[1] the infrared and raman spectra of the bismuth(III) oxide halides. J. Inorg. Nucl. Chem. 35, 1531–1534. https://doi.org/10.1016/0022-1902(73)80242-8.

Fan, W.J., Li, H.B., Zhao, X.J., Xiao, X.J., Huang, Y.C., Ji, H.B., Tong, Y.X., 2016. Boosting the photocatalytic performance of (001) BiOI: enhancing donor density and separation efficiency of photogenerated electrons and holes. Chem. Commun. (Camb.) 52, 5316–5319. https://doi.org/10.1039/C6CC00903D.

Geoking, C.F., Ghann, C.L., Wyatt, E.I., 1963. Chlorostannate method for separation of radiocesium. Anal. Chem. 35 (10), 1434–1436. https://doi.org/10.1021/ac60203a003.

Grote, R., Zhao, M., Shuller-Nickles, L., Amoroso, J., Gong, W., Lilova, K., Navrotsky, A., Tang, M., Brinkman, K.S., 2019. Compositional control of tunnel features in hollandite based ceramics: structure and stability of $(Ba,Cs)_{1.33}(Zn,Ti)_8O_{16}$. J. Mater. Sci. 54 (2), 1112–1125. https://doi.org/10.1007/s10853-018-2904-1.

Guy, C., Audubert, F., Lartigue, J.E., Latrille, C., Advocat, T., Fillet, C., 2002. New conditionings for separated long-lived radionuclides. C. R. Phys. 3 (4), 827–837. https://doi.org/10.1016/S1631-0705(02)01377-4.

Haefner, D.R., Tranter, T.J., 2007. Methods of Gas Phase Capture of Iodine from Fuel Reprocessing Off-gas: a Literature Survey. INL/EXT-07-12299, 2007. Available:. Idaho National Laboratory. https://inldigitallibrary.inl.gov/sites/sti/sti/3674601.pdf.

Kalaiselvan, S., Prasad, M.V.R., 1988. Some improvements in the estimation of 137Cs in urine by the AMP-chlorostannate method. J. Radioanal. Nucl. Chem. 125 (2), 431–437. https://doi.org/10.1007/BF02041700.

Krumhansl, J.L., Nenoff, T.M., 2011. Hydrotalcite-like layered bismuth-iodine-oxides as waste forms. Appl. Geochem. 26, 57–64. https://doi.org/10.1016/j.apgeochem.2010.11.003.

Lawter, A., Bonnett, J., Avalos, N., Canfield, N., Asmussen, R.M., 2019. Method Sensitivity Analysis for Iodine Waste Form Durability. PNNL-29098, prepared by. Pacific Northwest National Laboratory for the US Department of Energy, Washington DC.

Lee, W.E., Ojovan, M.I., Stennett, M.C., Hyatt, N.C., 2013. Immobilisation of radioactive waste in glasses, glass composite materials and ceramics. Advances in Applied Ceramics, Structural, Functional and Bioceramics 105 (1), 3–12. https://doi.org/10.1179/174367606X81669.

Luca, V., Drabarek, E., Griffith, C.S., Chronis, H., 2004. The immobilization of Cesium and Strontium in ceramic materials derived from tungstate sorbents. Mater. Res. Soc. Symp. Proc. 807, 1–6. https://doi.org/10.1557/PROC-807-303.

Luca, V., Cassidy, D., Drabarek, E., Murray, K., 2005. Cesium extraction from $Cs_{0.8}Ba_{0.4}Ti_8O_{16}$ hollandite nuclear waste form ceramics in nitric acid solutions. J. Mater. Res. 20 (6), 1436–1446. https://doi.org/10.1557/JMR.2005.0204.

Maddrell, E.R., Vance, E.R., Grant, C., Aly, Z., Stopic, A., Palmer, T., Harrison, J., Gregg, D.J., 2019. Silver iodide sodalite-wasteform/Hip canister interactions and aqueous durability. J. Nucl. Mater. 517, 71–79. https://doi.org/10.1016/j.jnucmat.2019.02.002.

Matyas, J., Fryxell, G.E., Busche, J., Wallace, K., Fifield, L.S., 2011. Functionalized silica aerogels: advanced materials to capture and immobilize radioactive iodine. Ceramic Engineering and Science Proceedings American Ceramic Society 32 (9), 21–32. https://doi.org/10.1002/9781118095386.ch3.

Moore, R.C., Pearce, C.I., Morad, J.W., Chatterjee, S., Levitskaia, T.G., Asmussen, R.M., Lawter, A.R., Neeway, J.J., Qafuku, N.P., Rigali, M.J., Saslow, S.A., Szecsody, J.E., Thallapally, P.K., Wang, G.H., Freedman, V.L., 2019. Iodine immobilization by materials through sorption and redox-driven processes: a literature review. Sci. Total Environ. 716, 1–11. https://doi.org/10.1016/j.scitotenv.2019.06.166.

Muller, I.S., McKeown, D.A., Pegg, I.L., 2014. Structure behavior of Tc and I ions in nuclear waste glass. Procedia Mater. Sci. 7, 53–59. https://doi.org/10.1016/j.mspro.2014.10.008.

Muresan, T.S., Vandenborre, J., Abdelouas, A., Grambow, B., Utsunomiya, S., 2011. Studies of (Cs,Ba)-hollandite dissolution under gamma irradiation at 95°C and at pH 2.5, 4.4 and 8.6. J. Nucl. Mater. 419, 281–290. https://doi.org/10.1016/j.jnucmat.2011.09.001.

Ojovan, M.I., Varlackova, G.A., Golubeva, Z.I., Burlaka, O.N., 2011. Long term field and laboratory leaching tests of cemented radioactive wastes. J. Hazard. Mater. 187, 296–302. https://doi.org/10.1016/j.jhazmat.2011.01.004.

Riley, B.J., Vienna, J.D., Strachan, D.M., McCloy, J.S., Jerden, J.R.J.L., 2016. Materials and processes for the effective capture and immobilization of radioiodine: a review. J. Nucl. Mater. 470, 307–326. https://doi.org/10.1016/j.jnucmat.2015.11.038.

Riley, B.J., Kroll, J.A., Peterson, J., Matyas, J., Olszta, M.J., Li, X.H., Vienna, J., 2017. Silver loaded aluminosilicate aerogels as iodine sorbents. ACS Appl. Mater. Interfaces 9 (38), 32907–32919. https://doi.org/10.1021/acsami.7b10290.

Scott, S., 2017. Development of Materials for Advanced Nuclear Fuel Cycle Applications. Ph.D Dissertation Available:http://digitool.rpi.edu:1801/view/action/nmets.do?DOCCHOICE=178828.xml&dvs=1588997196236~903&locale=zh_CN&search_terms=&view_profile=user&adjacency=&VIEWER_URL=/view/action/nmets.do?&DELIVERY_RULE_ID=2&divType=&usePid1=true&usePid2=true&COPYRIGHTS_DISPLAY_FILE=ETD01_thesis_copyrigh. Rensselaer Polytechnic Institute. t.

Scott, S.M., Hu, T., Yao, T.K., Xin, G.Q., Lian, J., 2015. Graphene based sorbents for I-129 capture and sequestration. Carbon. 90, 1–8. https://doi.org/10.1016/j.carbon.2015.03.070.

Sinha, P.K., Panicker, P.K., Amalraj, R.V., Krishnasamy, V., 1995. Treatment of radioactive liquid waste containing caesium by indigenously available synthetic zeolites: a comparative study. Waste Manag. 15 (2), 149–157. https://doi.org/10.1016/0956-053X(95)00014-Q.

Sun, Q.H., Xu, Y.D., Zhang, H.J., Xiao, B., Liu, X., Dong, J.P., Cheng, Y.B., Zhang, B.B., Jie, W.Q., Kanatzdis, M.G., 2018. Optical and electronic anisotropies in perovskitoid crystals of $Cs_3Bi_2I_9$ studies of nuclear radiation detection. J. Mater. Chem. A 6,

23388–23395. https://doi.org/10.1039/C8TA09525F.
Tanabe, H., Sakuragi, T., Yamaguchi, K., Sato, T., Owada, H., 2010. Development of new waste forms to immobilize iodine-129 released from a spent fuel reprocessing plant. Adv. Sci. Technol. 73, 158–170. https://doi.org/10.4028/www.scientific.net/AST.73.158.
Tumurugoti, P., Sundaram, S.K., Misture, S.T., 2018. Cesium immobilization in (Ba,Cr)-hollandites: effects on structure. J. Solid State Chem. 258, 72–78. https://doi.org/10.1016/j.jssc.2017.10.008.
U.S.E.P.A, 2012. Identification and listing of hazardous waste. In: In: Agency, E.P. (Ed.), CFR 261 Vol. 40 Environmental Protection Agency, Washington, D.C Available: https://archive.epa.gov/wastes/conserve/materials/usedoil/web/xml/cfr-2012-title40-vol27-part261.xml.
Uno, M., Shinohara, M., Kurosaki, K., Yamanaka, S., 2001. Some properties of a lead vanado-iodoapatite $Pb_{10}(VO_4)_6I_2$. J. Nucl. Mater. 294, 119–122. https://doi.org/10.1016/S0022-3115(01)00462-7.
Vinokurov, S.E., Kulyako, Y.M., Slyunchev, O.M., Rovnyi, S.I., Wagh, A.S., Maloney, M.D., Myasoedov, B.F., 2009. Magnesium potassium phosphate matrices for immobilization of high-level liquid wastes. Radiochemistry 51 (1), 65–72. https://doi.org/10.1134/S1066362209010159.
Wagh, A.S., Sayenko, S.Y., Shkuropatenko, V.A., Tarasov, R.V., Dykiy, M.P., Svitlychniy, Y.O., Virych, V.D., Ulybkina, E.A., 2016. Experimental study on cesium immobilization in struvite structures. J. Hazard. Mater. 302, 241–249. https://doi.org/10.1016/j.jhazmat.2015.09.049.
Weissbart, E.J., Rimstidt, J.D., 2000. Wollastonite: incongruent dissolution and leached layer formation. Geochim. Cosmochim. Acta 64 (23), 4007–4016. https://doi.org/10.1016/S0016-7037(00)00475-0.
Yanagisawa, K., Nishioka, M., Yamasaki, N., 1987. Immobilization of Cesium into pollucite structure by hydrothermal hot-pressing. J. Nucl. Sci. Technol. 24 (1), 51–60. https://doi.org/10.1080/18811248.1987.9735774.
Yang, J.H., Park, H.S., Cho, Y.Z., 2017. Silver phosphate glasses for immobilization of radioactive iodine. Ann. Nucl. Energy 110, 208–214. https://doi.org/10.1016/j.anucene.2017.06.042.
Zhang, Z., Heath, A., Valsaraj, K.T., Ebert, W., Yao, T., Lian, J., Wang, J., 2018a. Mechanism of iodine release from iodoapatite in aqueous solution. RSC Adv. 8, 3951–3957. https://doi.org/10.1039/C7RA11049A.
Zhang, H.J., Xu, Y.D., Sun, Q.H., Dong, J.P., Lu, Y.F., Zhang, B.B., Jie, W.Q., 2018b. Lead free halide pervoskite $Cs_3Bi_2I_9$ bulk crystals grown by a low temperature solution method. Cryst. Eng. Comm. 20, 4935–4941. https://doi.org/10.1039/C8CE00925B.
Zhu, W.G., Xin, G.Q., Scott, S.M., Xu, W.Q., Yao, T.K., Gong, B.W., Wang, Y.C., Li, M.X., Lian, J., 2019. Deciphering the degradation mechanism of the lead-free all inorganic perovskite Cs_2SnI_6. Npj Mater. Degrad. 3, 1–7. https://doi.org/10.1038/s41529-019-0068-3.